# Supporting Information

## Plasma-induced implanting of active species in metal-organic frameworks for efficient hydrogen evolution reaction

Qi Qi[a†], Duo Shao[a†], Yitong Zhou[a], Qi Wang[a]* and Xin-Yao Yu[a,b]*

[a]Institutes of Physical Science and Information Technology

Anhui University

Hefei 230601, P. R. China

[b]School of Materials Science and Engineering

Anhui University

Hefei 230601, P. R. China

[†]These two authors contribute equally to this work.

***Corresponding Authors**

*Email: yuxinyao@ahu.edu.cn

*Email: wangqi@ahu.edu.cn

***Chemicals**:*

Peruliphthalic acid (PTA, 99%) was purchased from Macklin Biochemical Corporation Ltd. Nickel chloride hexahydrate ($NiCl_2 \cdot 6H_2O$, AR), ammonium molybdate ($(NH_4)_2MoO_4$, AR) N,N-dimethylformamide (DMF, AR), hydrochloric acid (HCl, AR), acetone (AR), and anhydrous ethanol (AR) were purchased from Sinopill Chemical Reagent Co., LTD. Ni foam (thickness: 1.5 mm) was purchased from Taiyuan Liyuan Lithium Technology Co., LTD. and the water used was deionized water (DIW). All chemicals were used as obtained without further purification.

***Pre-treatment of Ni foam*:**

A piece of nickel foam (3 cm×3 cm) was successively cleaned in 1.0 M HCl solution, deionized water, and ethanol with each ultrasonication for 10 min and finally dried in a 70 ℃ oven.

***Synthesis of Ni MOF/POM and Ni MOF***:

In a typical synthesis, 1 mmol of nickel chloride ($NiCl_2 \cdot 6H_2O$), 1 mmol of terephthalic acid (PTA), and 0.1 mmol of ammonium molybdate ($(NH_4)_2MoO_4$) were dissolved in a mixed solution composed of 35 mL of DMF, 2.5 mL of ethanol, and 2.5 mL of deionized water. And then the mixture was transferred into a 100 mL PTFE liner. After immersing one piece of Ni foam into the mixed solution, the PTFE liner was heated in an oven at 125℃ for 12 h. After naturally cooled down to room temperature, the postreaction foam was carefully washed several times with deionized water and absolute ethanol with the assistance of ultrasound to obtain Ni MOF/POM. The Ni MOF was synthesized when $(NH_4)_2MoO_4$ was not added. To investigate the effect of Mo-incorporated amount, the amount of ammonium molybdate used was changed to 0.05 mol and 0.15 mol without changing other reaction conditions. The samples synthesized with the addition of 0.05 mol and 0.15 mol of $(NH_4)_2MoO_4$ were named as

Ni MOF/POMs-1 and Ni MOF/POM-2, respectively.

***Synthesis of the P-Ni MOF/POM and P-Ni MOF*:**

The as-synthesized Ni MOF/POM and Ni MOF were put into a radio frequency (RF) plasma enhanced chemical vapor deposition (PECVD) device for activation. The gas ratio of $H_2/N_2$ is 1:9 and the total gas pressure is 50 Pa. The RF power was set to 400 W and the activation time was 20 min. After plasma activation, the P-Ni MOF/POM and P-Ni MOF were then obtained. The plasma-activated Ni MOF/POMs-1 and Ni MOF/POM-2 with the same plasma parameter as that of P-Ni MOF/POM were denoted as P-Ni MOF/POMs-1 and P-Ni MOF/POM-2, respectively. When investigating the plasma atmosphere effect, Ni MOF/POM and Ni MOF were activated in sole $N_2$ or $H_2$ plasma (gas pressure: 50 Pa, RF power: 400 W, activation time: 20 min). The $N_2$ and $H_2$ plasma-activated Ni MOF/POM were named as P-Ni MOF/POM-$N_2$ and P-Ni MOF/POM-$H_2$, respectively. The $N_2$ and $H_2$ plasma-activated Ni MOF are named as P-Ni MOF-$N_2$ and P-Ni MOF-$H_2$, respectively. The plasma activated Ni MOF/POM obtained at the gas pressure of 30 Pa and 70 Pa with plasma power and reduction time unchanged (400 W and 20 min) were labeled as P-Ni MOF/POM-30 Pa and P-Ni MOF/POM-70 Pa, respectively. The plasma activated Ni MOF/POM with processing time of 10 min and 30 min with plasma power and gas pressure unchanged (400 W and 50 Pa) were named as P-Ni MOF/POM-10 min and P-Ni MOF/POM-30 min, respectively.

***Fabrication of Pt/C electrode*:**

5 mg of commercial Pt/C powder (20 wt%) was dispersed in a mixed solution of ethanol (270 μL), deionized water (200 μL), and Nafion solution (30 μL) in 1 mL of centrifuge tube. After ultrasonic treatment for 30 min, the turbid liquid was dropped onto Ni foam and dried out. The mass loading of Pt/C on Ni foam was 2 $mg \cdot cm^{-2}$.

***Material characterizations**:*

The morphology of the catalyst was characterized by scanning electron microscopy (SEM, Hitachi S-4800) and transmission electron microscope (TEM, JEOL Japan Electronics Co., Ltd JEM-2100F). The crystal structure of the catalyst was characterized by X-ray diffraction instrument (XRD, BRUKER D2phaser). The surface elements, chemical valence states, and relative content of the catalyst were characterized by X-ray photoelectron spectroscopy (XPS, Thermo Fisher Scientific ESCALAB250). The Fourier transform infrared spectrum (FT-IR) was recorded on the Thermo Fisher Scientific Nicoletis 50. Gas chromatography (GC9790) was used to monitor the hydrogen production. The optical emission signal of the plasma was analyzed by a high speed spectrometer (PG2000, Idea Optics). The water droplet contact angle was measured on a contact angle measuring instrument (KRUSS Scientific DSA25E-30010795). The Raman spectra of the electrocatalyst were measured by Thermo Fisher Scientific DXR Smart Raman and the wavelength of the used laser was 532 nm.

***Electrochemical characterizations:***

All electrochemical test data were tested on the CHI760E electrochemical workstations and Biologic multi-channel potentiostat (MPG-2) in a three-electrode system. Hg/HgO is used as the reference electrode, the carbon rod is the counter electrode, and the prepared sample is the working electrode. The alkaline seawater was formulated by mixing the KOH solution with the natural seawater and adjusting the pH of the mixed electrolyte to 14. No other pretreatment was performed after natural seawater filtration. The potentials referred to herein are all relative to the reversible hydrogen electrode (RHE).

During the HER test, the scan rate of the linear scan voltammetric (LSV) curves

was 1 mV $s^{-1}$ and potential interval was from 0.02 V to 0.6 V *vs*. RHE. Tafel slope values were obtained by logarithmic fitting of the hydrogen polarization curve by the Tafel equation: $\eta = b\log(j) + a$. Electrochemical impedance (EIS) is tested by AC impedance spectroscopy with a frequency range from $10^6$ to 0.005 Hz. The electrochemical active area (ECSA) of the catalyst is assessed by its double-layer capacitance ($C_{dl}$). A series of cyclic voltammetric (CV) curves at different sweeps (20, 40, 60, 80, and 100 $mVs^{-1}$) were obtained within the potential interval from 0.05 V to 0.15 V *vs*. RHE. The chronoamperometry (CA) at a constant potential was used to test the stability of the catalysts. The TOF could be calculated by the following formula: $TOF = I/2NF$, where $F$ is the Faraday constant (96485 C $mol^{-1}$). $N$ represents the number of active sites, obtained by the following formula: $N = Q/2F = (It)/2F = (IV/\mu)/2F = S/(2F\mu)$, where $S$ represents the effective area obtained after integrating the CV curve and $\mu$ represents the sweep. The actual amount of $H_2$ generated on the working electrode is directly obtained by gas chromatography: $n(H_2)_{exp} = x_o \times n$, where $x_o$ represents the amount of hydrogen generated (mol $ppm^{-1}$) and $n$ refers to the amount of hydrogen produced in 1 $cm^3$. The amount of $H_2$ produced theoretically during the HER process is obtained by the following formula: $n(H_2)_{tho} = It/2F$. The calculation equation for Faraday efficiency is as follows: $FE = n(H_2)_{exp}/n(H_2)_{tho} \times 100\%$.

In the in-situ Raman test, the nickel foam grown with catalysts was used as the working electrode. The Hg/HgO electrode and graphite rod were employed as the reference electrode and electrode, respectively. 1 M KOH was used as the electrolyte. The in-situ electrochemical test was conducted in homemade electrolysis cell. During the in situ test, the laser point is aligned at the nickel foam and an electrical signal is applied to the nickel foam to obtain real-time Raman spectrum. In situ Raman data are obtained from LSV measurements with a scan rate of 1 mV $s^{-1}$ and a scan range from 0

to 0.5 V *vs*. RHE. Kinetic isotope effect (KIE) test was performed in 1 M NaOH/$H_2O$ and 1 M NaOD/$D_2O$ solutions. The following formula is used to calculate the KIE value: $KIE_{H/D} = (k_{H2O}/k_{D2O}) = (j_H/j_D)_\eta$, where $j_H$ is the corresponding current density at a $\eta$ overpotential in 1 M NaOH/$H_2O$ solution. The $j_D$ is the corresponding current density at a certain $\eta$ overpotential in the 1 M NaOD/$D_2O$ solution. Since the catalytic activity varies with the applied overpotential, the $j_H$ and $j_D$ should be compared at the same overpotential.

***Theoretical calculations:***

Density functional theory calculations were carried out using the Vienna Ab-initio Simulation Package (VASP)[1-3]. The Perdew-Burke-Ernzerh (PBE) in the generalized gradient approximation (GGA) was applied to describe the exchange-correlation function[4]. The interaction between electrons and ions was considered with the method of projector augmented wave (PAW)[5, 6]. Based on our careful convergence tests, the plane wave energy cutoff was set to 400 eV. The convergence criterion of electronic structure was set to $10^{-4}$ eV, and the atomic relaxation was continued until the forces acting on atoms were smaller than 0.05 eV/Å. The Brillouin-zone sampling were conducted using Monkhorst-Pack (MP) grids of special points with the separation of 0.04 $Å^{-1}$, and a Gaussian smearing of 0.05 eV was applied to speed up electronic convergence. The 4×4 supercell of Ni(111), 1×2 supercell of $Ni_3N$(110), 2×3 supercell of $MoNi_4$ (400), 3×3 supercell of $Ni(OH)_2$(001) with hydroxyl vacancy were used to build the calculation models. The optimized atomic configurations were illustrated with VESTA software[7].

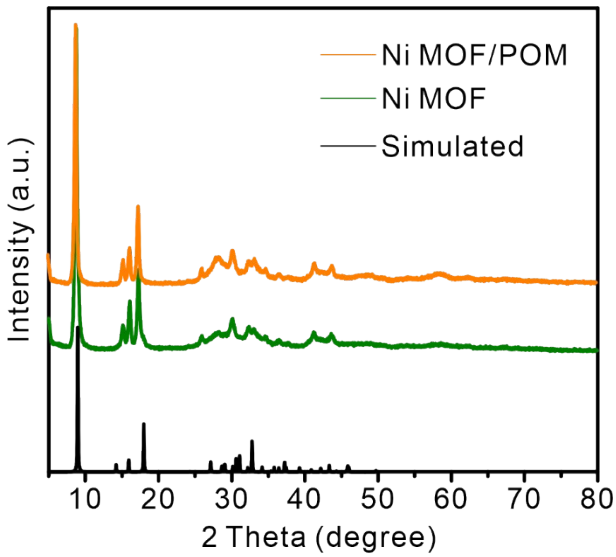


**Fig. S1.** XRD patterns of Ni MOF and Ni MOF/POM.

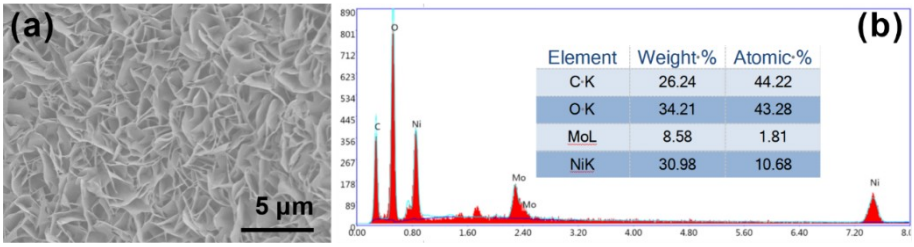


**Fig. S2.** (a) SEM image and (b) EDS spectrum of Ni MOF/POM.

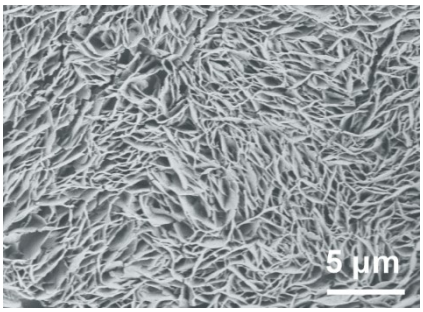


**Fig. S3.** SEM image of Ni MOF.

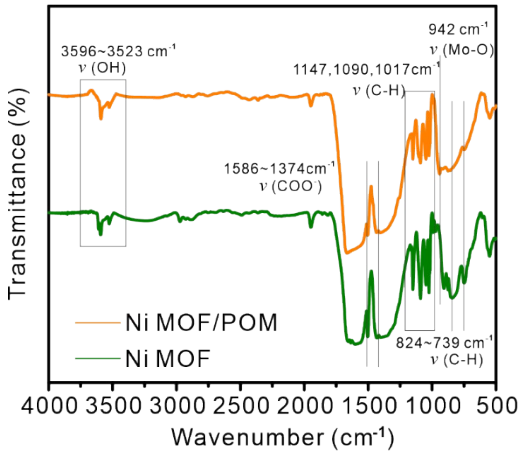


**Fig. S4.** FT-IR spectra of Ni MOF and Ni MOF/POM.

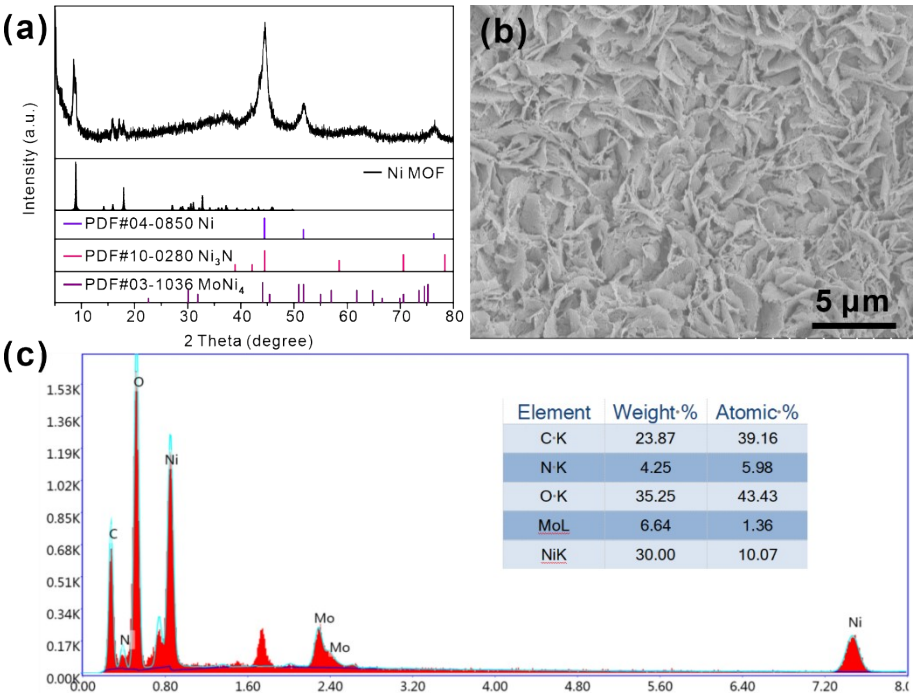


**Fig. S5.** (a) XRD pattern, (b) SEM image, and (c) EDS spectrum of P-Ni MOF/POM.

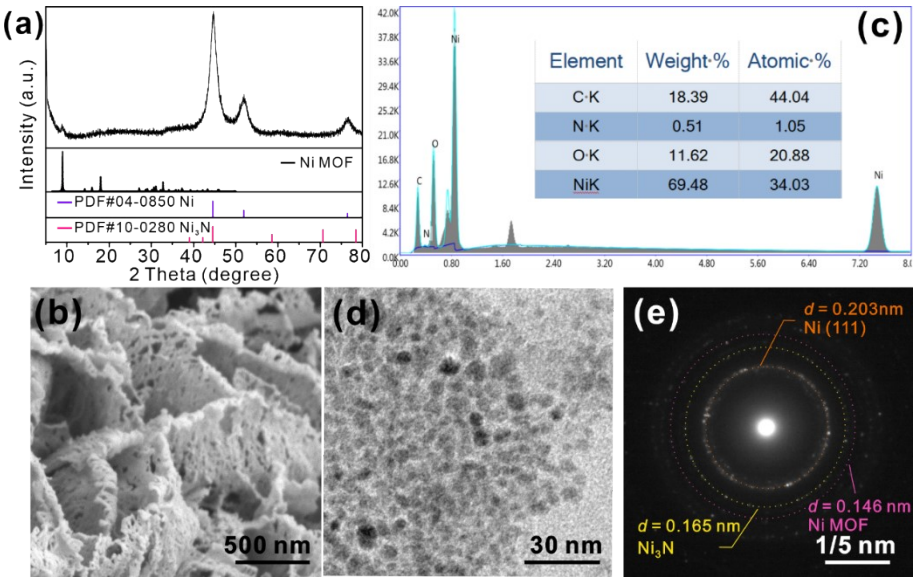


**Fig. S6.** (a) XRD pattern, (b) EDS spectrum, (c) SEM image, (d) TEM image, and (e) SAED pattern of P-Ni MOF.

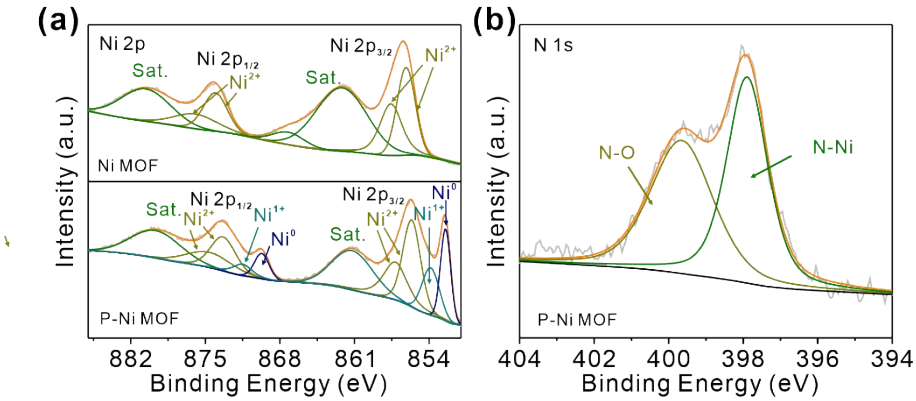


**Fig. S7.** The high-resolution (a) Ni 2p and (b) N1 s XPS spectra of Ni MOF and P-Ni MOF NSAs.

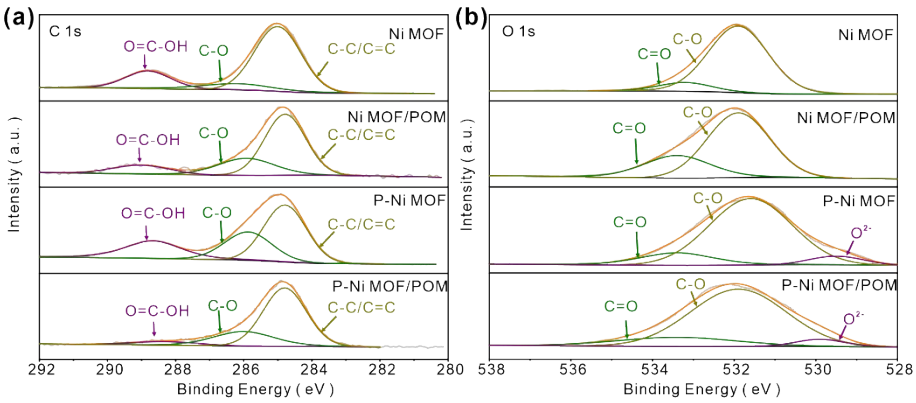


**Fig. S8.** The high-resolution (a) C 1s and (b) O 1s XPS spectra of Ni MOF, Ni MOF/POM, P- Ni MOF, and P- Ni MOF/POM.

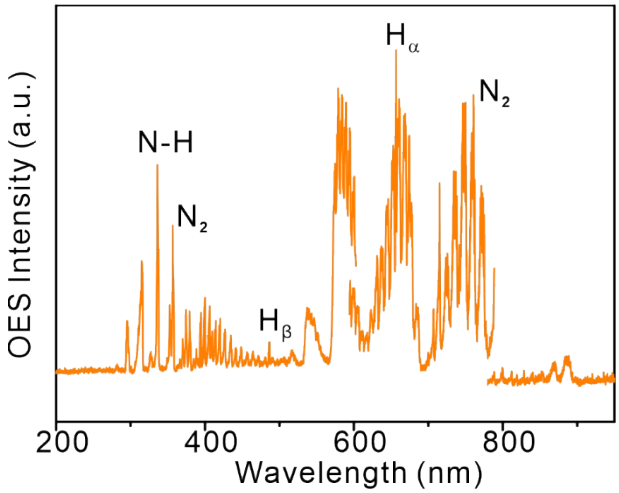


**Fig. S9.** OES of $N_2/H_2$ plasma.

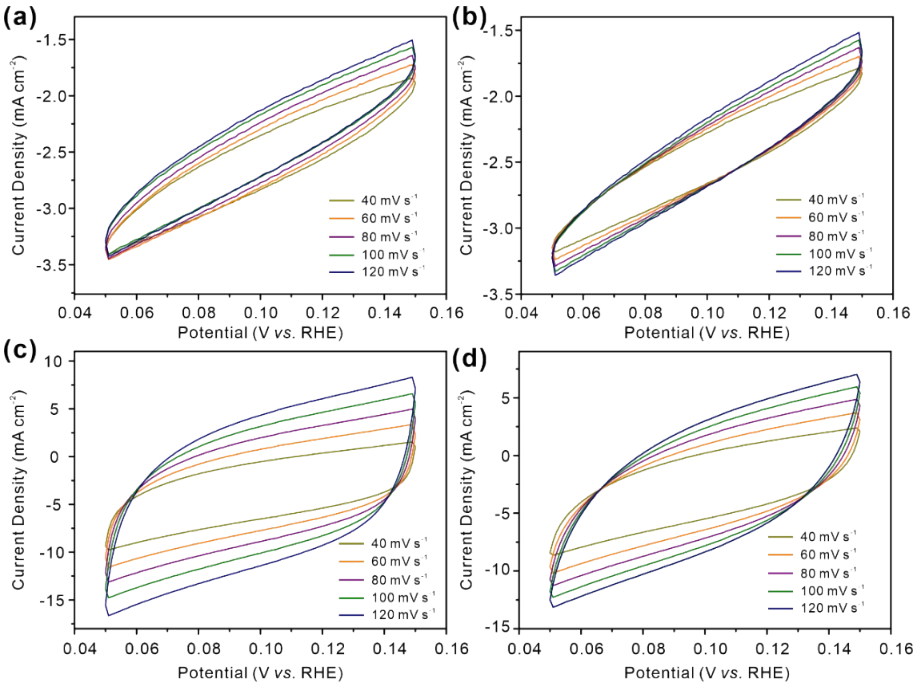


**Fig. S10.** CV curves of (a) Ni MOF, (b) Ni MOF/POM, (c) P- Ni MOF, and (d) P- Ni MOF/POM in the double layer capacitive region at different scan rates.

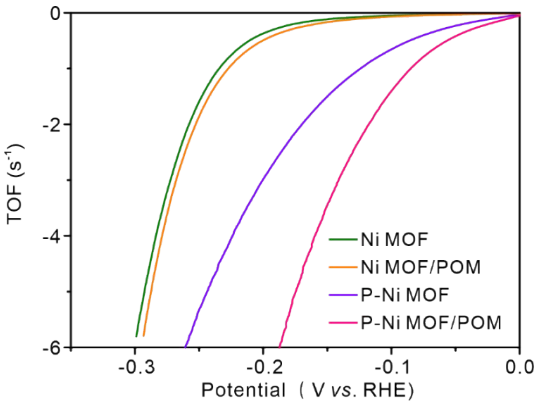


**Fig. S11.** TOF curves of Ni MOF, Ni MOF/POM, P-Ni MOF, and P-Ni MOF/POM.

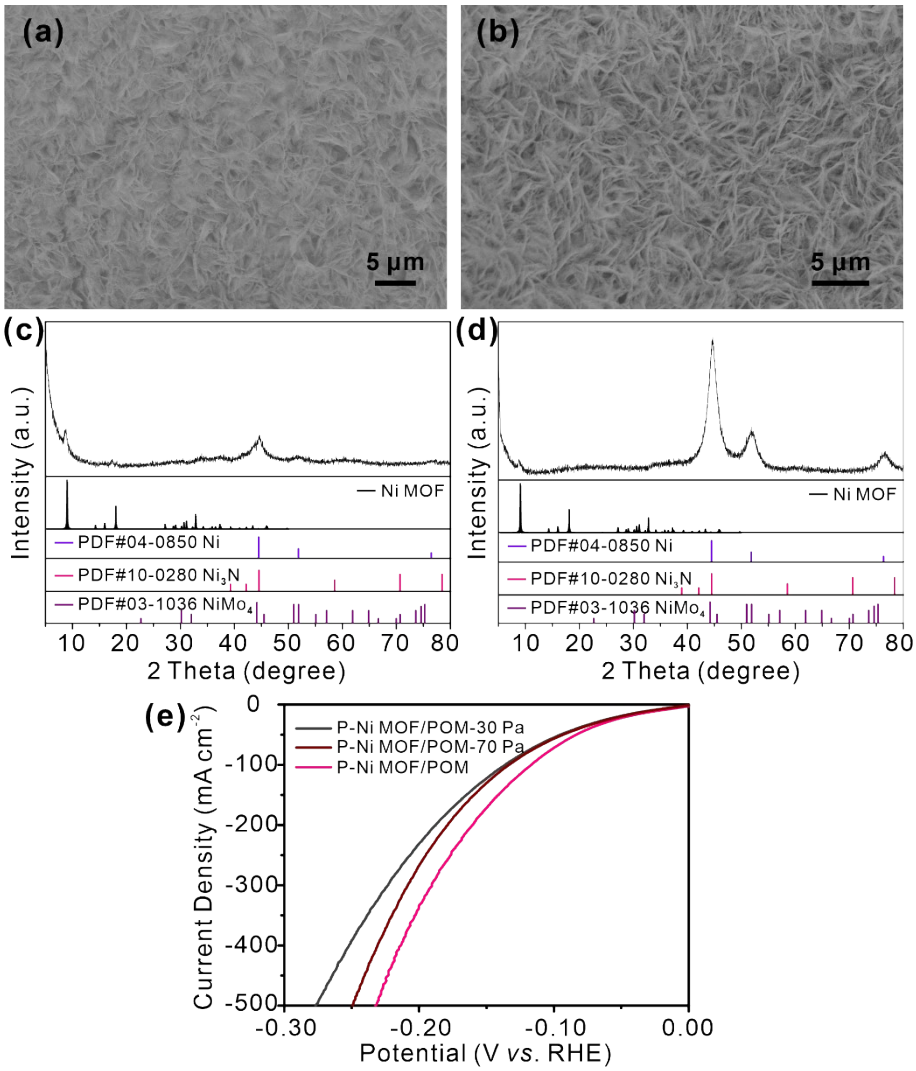


**Fig. S12.** (a) SEM image and (c) XRD pattern of P-Ni MOF/POM-30 Pa. (b) SEM image and (d) XRD pattern of P-Ni MOF/POM-70 Pa. (c) Polarization curves of P- Ni MOF/POM-30 Pa, P-Ni MOF/POM (the sample synthesized at 50 Pa), and P-Ni MOF/POM-70 Pa.

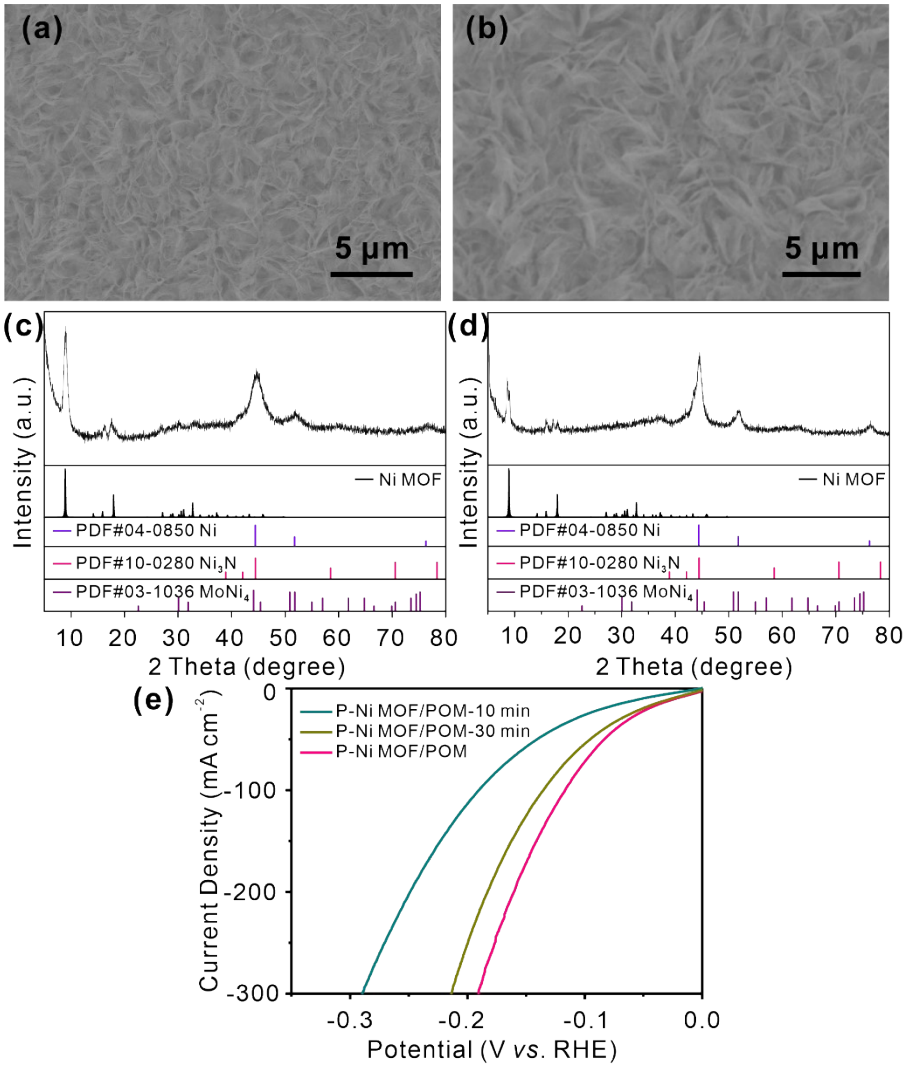


**Fig. S13.** (a) SEM image and (c) XRD pattern of P-Ni MOF/POM-10 min. (b) SEM image and (d) XRD pattern of P-Ni MOF/POM-30 min. (c) Polarization curves of P-Ni MOF/POM-10 min, P-Ni MOF/POM (the sample obtained with plasma processing time of 20 min), and P-Ni MOF/POM-30 min.

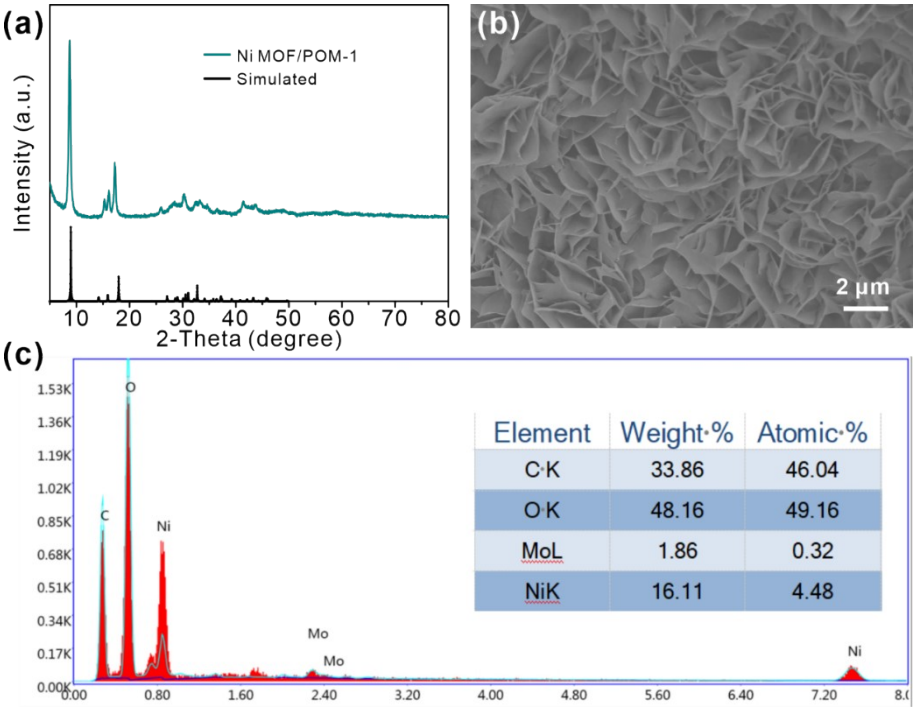


**Fig. S14.** (a) XRD pattern, (b) SEM image, and (c) EDS spectrum of Ni MOF/POM-1.

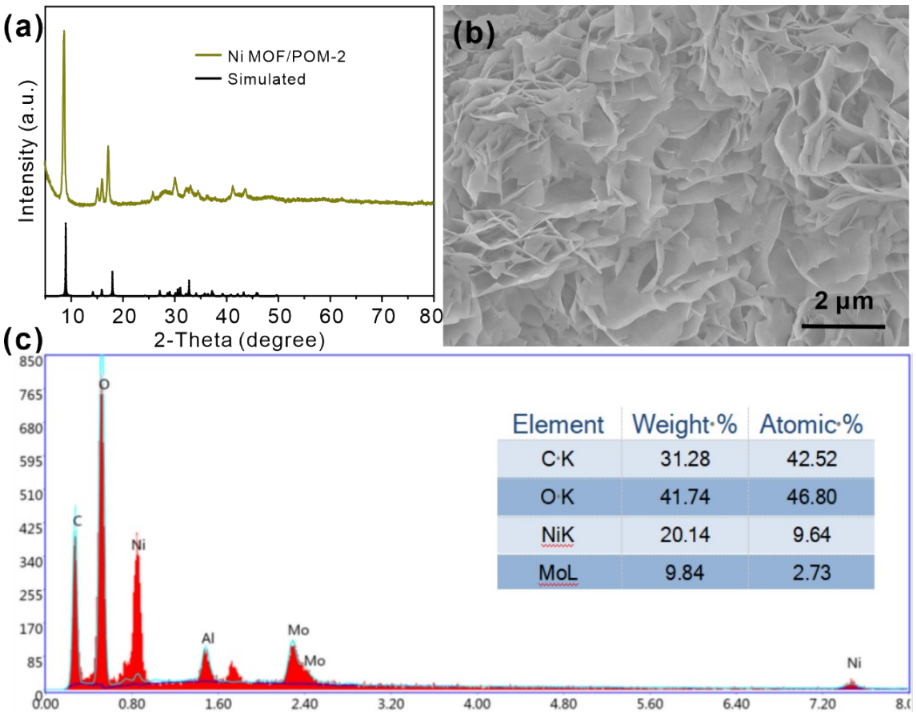


**Fig. S15.** (a) XRD pattern, (b) SEM image, and (c) EDS spectrum of Ni MOF/POM-2.

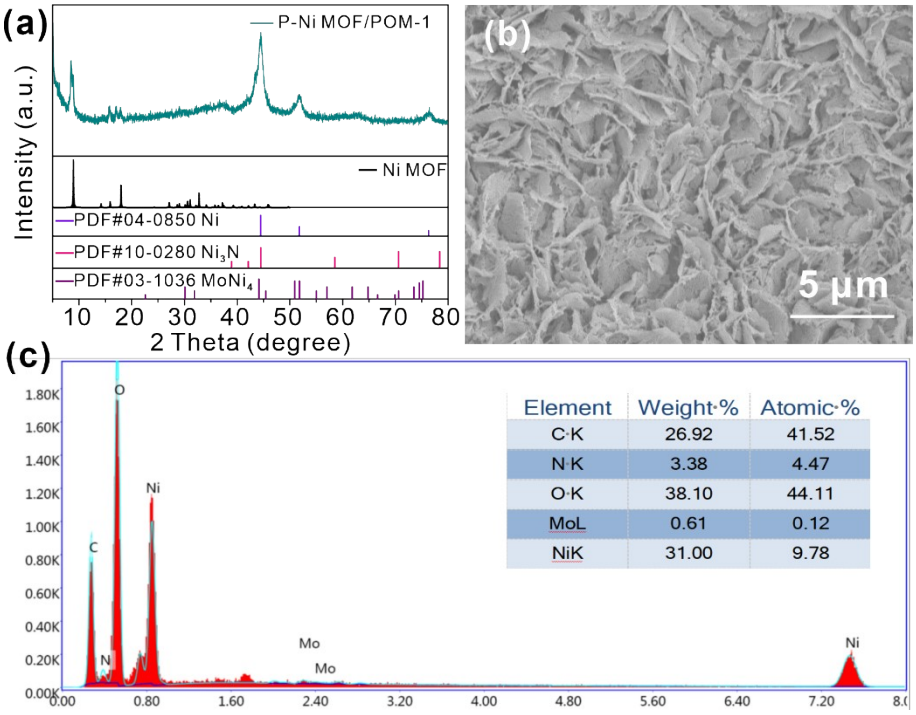


**Fig. S16.** (a) XRD pattern, (b) SEM image, and (c) EDS spectrum of P-Ni MOF/POM-1.

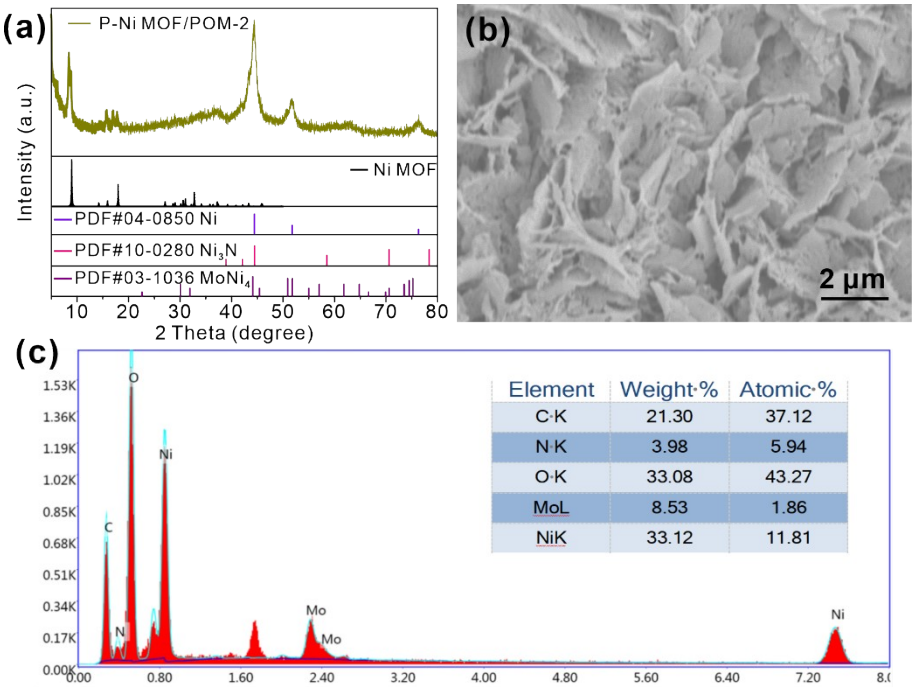


**Fig. S17.** (a) XRD pattern, (b) SEM image, and (c) EDS spectrum of P-Ni MOF/POM-2.

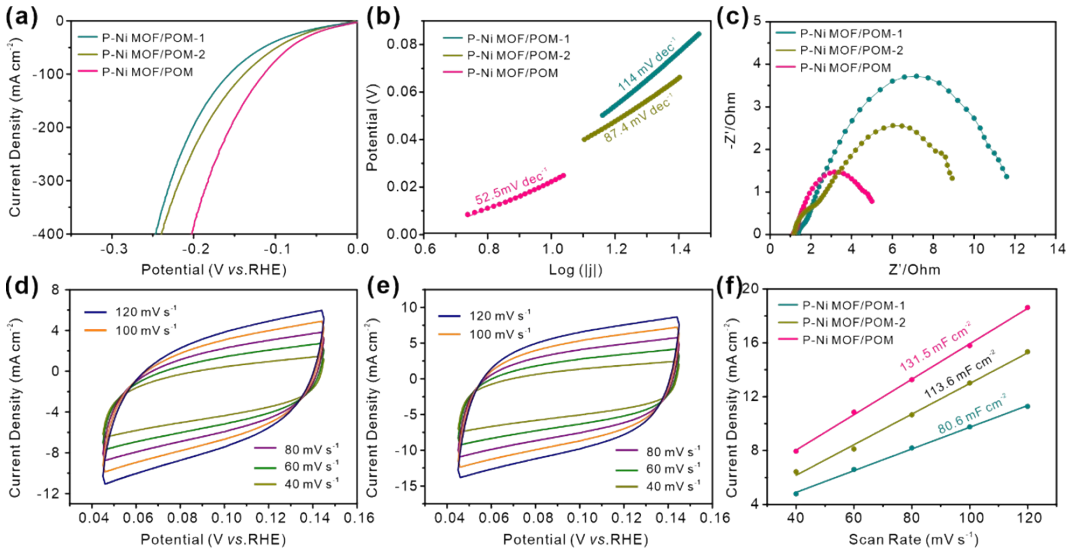


**Fig. S18.** (a) LSV curves, (b) Tafel plots, and (c) Nyquist plots of P-Ni MOF/POM-1, P-Ni MOF/POM, and P-Ni MOF/POM-2. CV curves of (d) P-Ni MOF/POM-1 and (e) P-Ni MOF/POM-2 NSAs in the double layer capacitive region at different scan rates. (f) Current density differences plotted against scan rates of P-Ni MOF/POM-1, P-Ni MOF/POM, and P- Ni MOF/POM-2 NSAs.

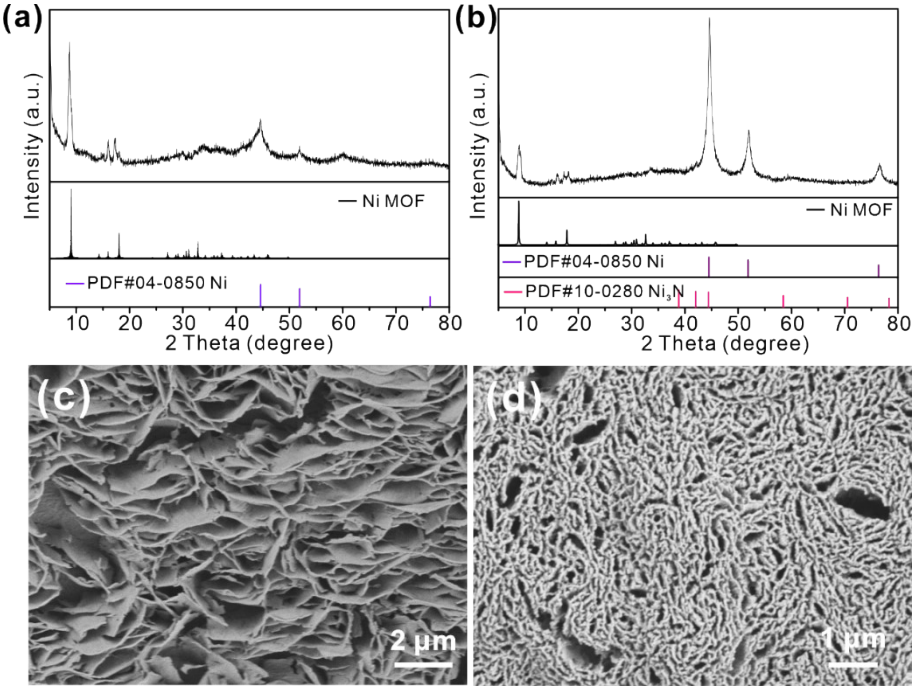


**Fig. S19.** XRD patterns and SEM images of (a, c) P- Ni MOF-$H_2$ and (b, d) P-Ni MOF-$N_2$.

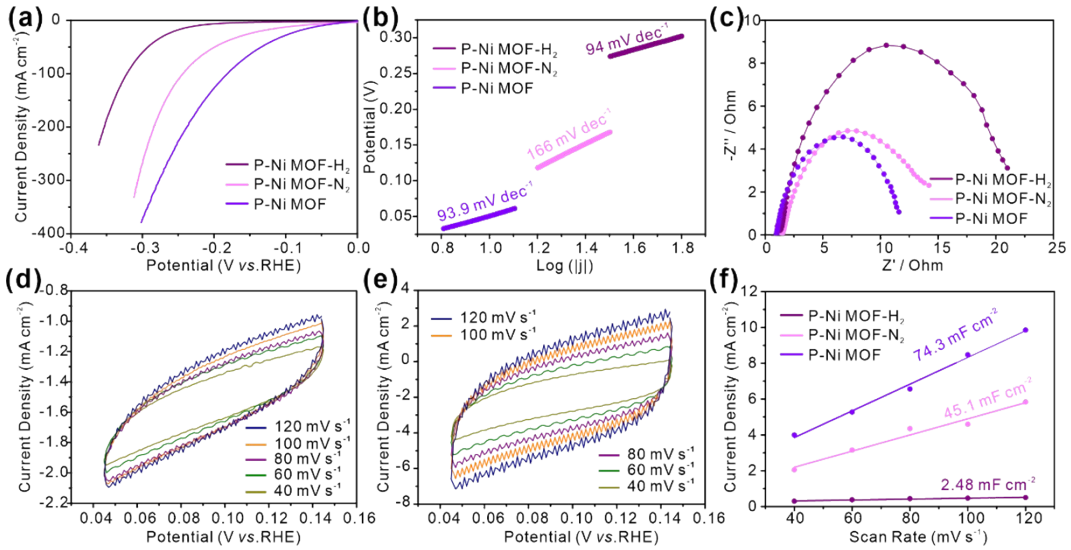


**Fig. S20.** (a) LSV curves, (b) Tafel plots, and (c) Nyquist plots of P-Ni MOF-$H_2$, P-Ni MOF-$H_2$, and P-Ni MOF. (d) CV curves of (d) P-Ni MOF-$H_2$ and (e) P-Ni MOF-$N_2$ in the double layer capacitive region at different scan rates. (f) Current density differences plotted against scan rates of P-Ni MOF-$H_2$, P-Ni MOF-$N_2$, and P-Ni MOF.

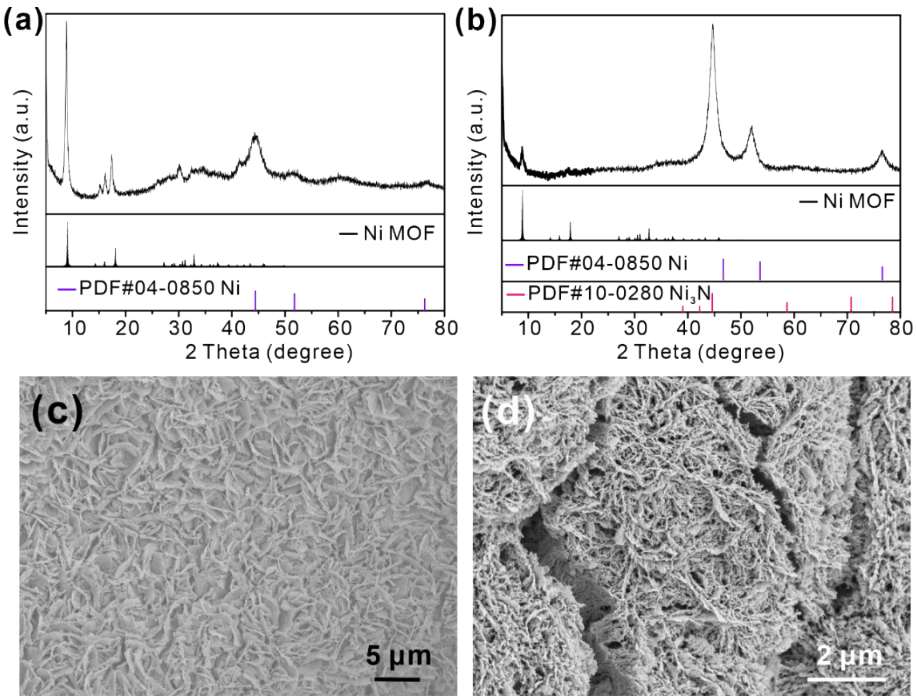


**Fig. S21.** XRD patterns and SEM images of (a,c) P-Ni MOF/POM-$H_2$ and (b,d) P-Ni MOF/POM-$N_2$.

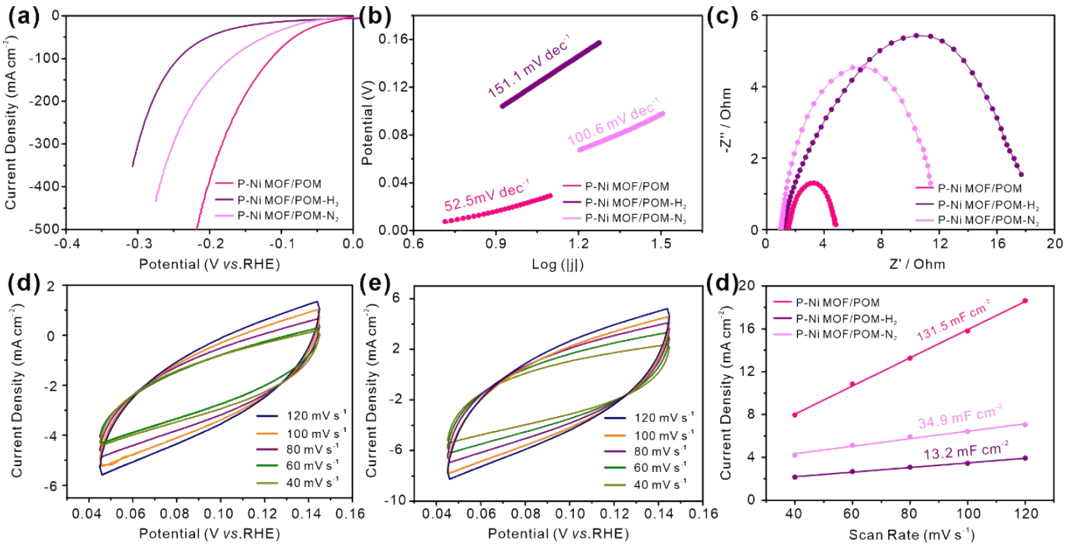


**Fig. S22.** (a) LSV curves, (b) Tafel plots, and (c) Nyquist plots of P-Ni MOF/POM-$H_2$, P-Ni MOF/POM-$N_2$, and P- Ni MOF/POM. (d) CV curves of (d) P-Ni MOF/POM-$H_2$ and (e) P-Ni MOF/POM-$N_2$ in the double layer capacitive region at different scan rates. (f) Current density differences plotted against scan rates of P-Ni MOF/POM-$H_2$, P-Ni MOF/POM-$N_2$, and P-Ni MOF/POM.

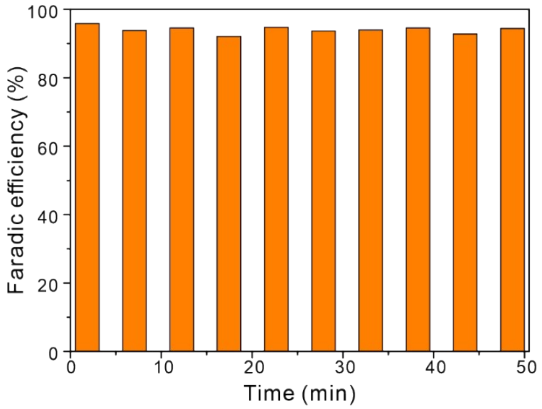


**Fig. S23.** FE for hydrogen evolution on P-Ni MOF/POM as a function of time at the current density of 10 mA $cm^{-2}$.

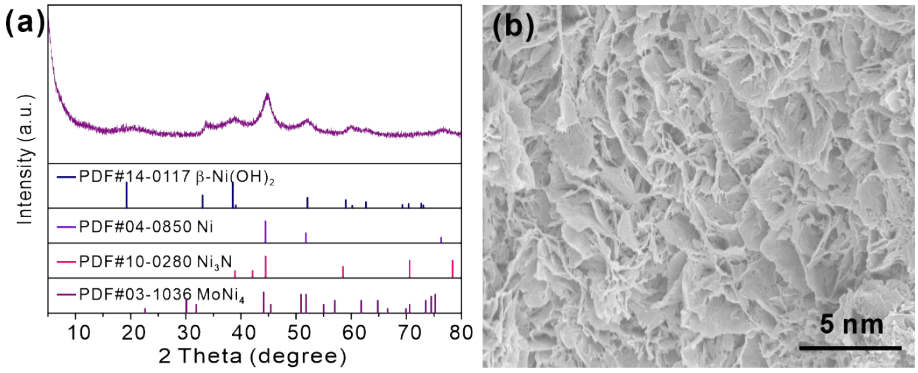


**Fig. S24.** (a) XRD pattern and (b) SEM image of P-Ni MOF/POM after stability test.

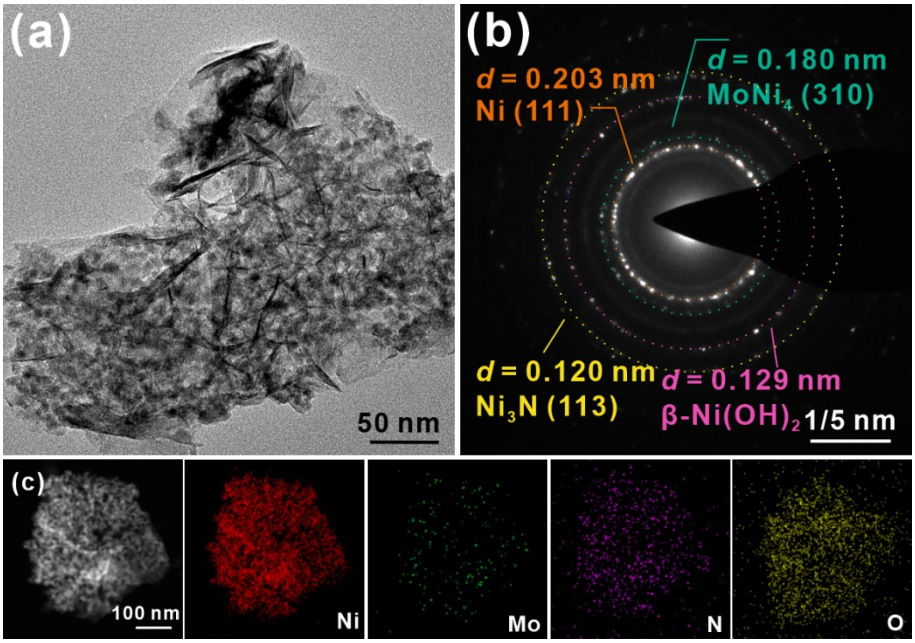


**Fig. S25.** (a) TEM image, (b) SAED pattern, and (d) EDX elemental mapping images of P-Ni MOF/POM after stability test.

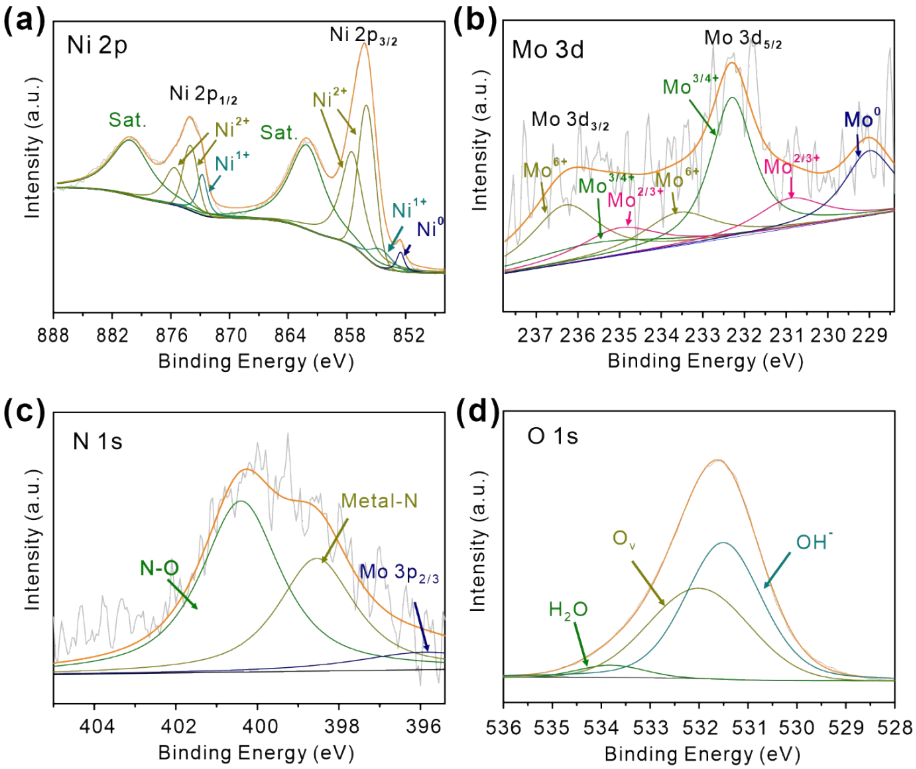


**Fig. S26.** The high-resolution (a) Ni 2p, (b) Mo 3d, (c) N 1s and (d) O 1s XPS spectra of P-Ni MOF/POM after stability test.

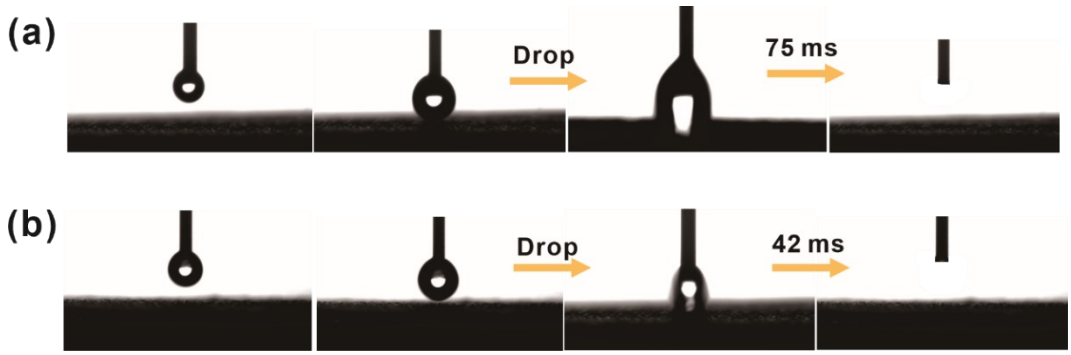


**Fig. S27.** Dynamic contact angles of (a) Ni MOF and (b) P-Ni MOF.

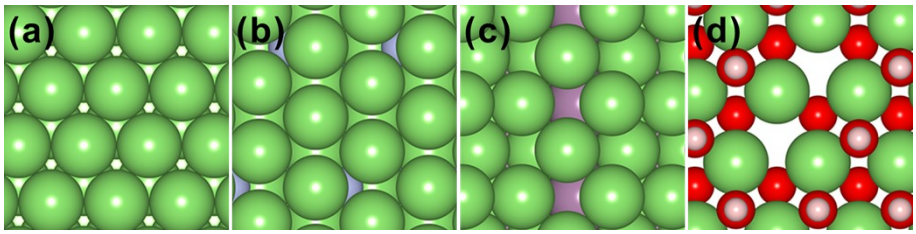


**Fig. S28.** Top view of the (a) Ni, (b) $Ni_3N$, (c) $MoNi_4$, and (d) $\beta$-$Ni(OH)_2$. The pink, green, gray, purple, and red spheres represent H, Ni, N, Mo, and O atoms, respectively.

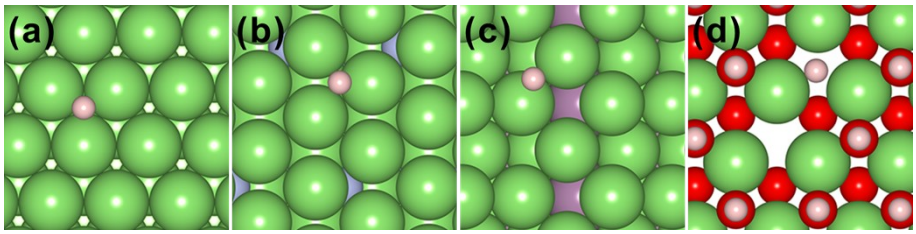


**Fig. S29.** Top view of *H adsorption on the (a) Ni, (b) $Ni_3N$, (c) $MoNi_4$, and (d) $\beta$-$Ni(OH)_2$. The pink, green, gray, purple and red spheres represent H, Ni, N, Mo, and O atoms, respectively.

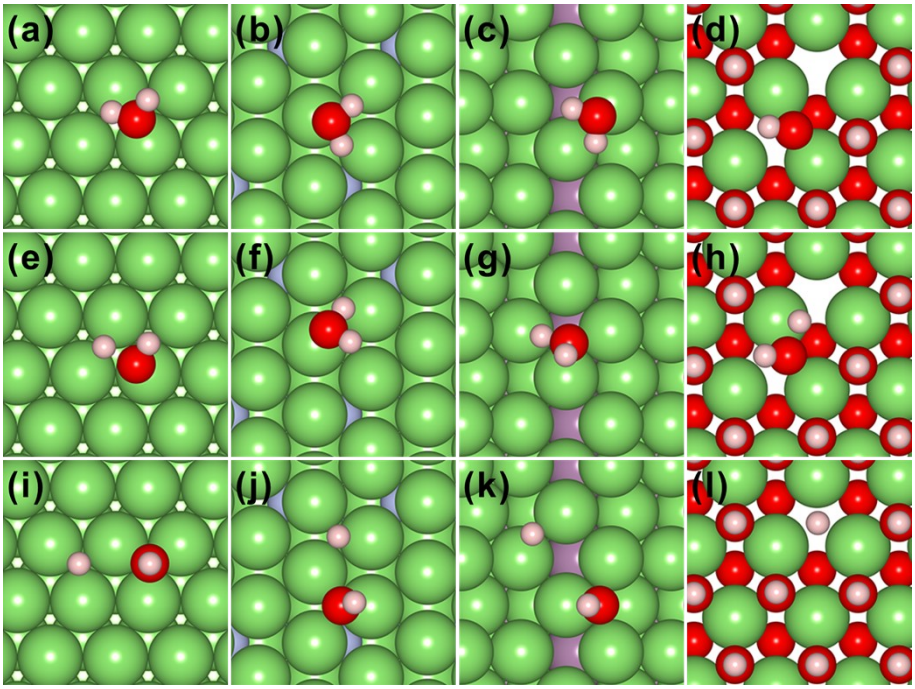


**Fig. S30.** Top views of (a) $H_2O$*, (e) OH-H*, and (i) OH* + H* on Ni. Top views of (b) $H_2O$*, (f) OH-H*, and (j) OH* + H* on $Ni_3N$. Top views of (c) $H_2O$*, (g) OH-H*, and (k) OH* + H* on $MoNi_4$. Top views of (d) $H_2O$*, (h) OH-H*, and (l) OH* + H* on $\beta$-$Ni(OH)_2$. The pink, green, gray, purple and red spheres represent H, Ni, N, Mo, and O atoms, respectively.

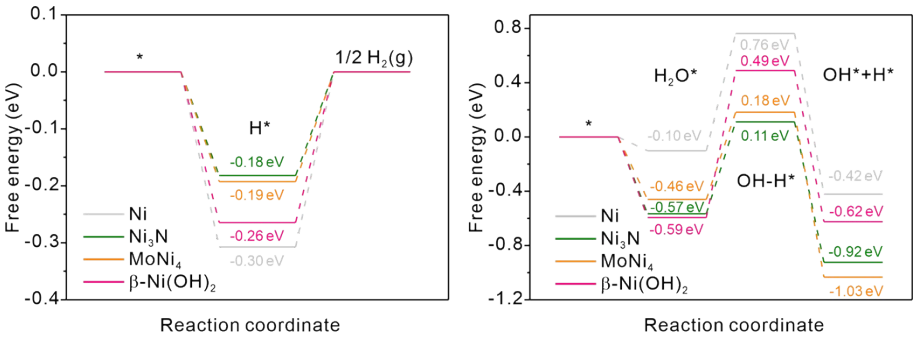


**Fig. S31.** (a) Free energy diagrams for hydrogen adsorption and (b) the relative energy diagram of the water adsorption and dissociation path on metallic Ni, $Ni_3N$, $MoNi_4$, and $\beta$-$Ni(OH)_2$.

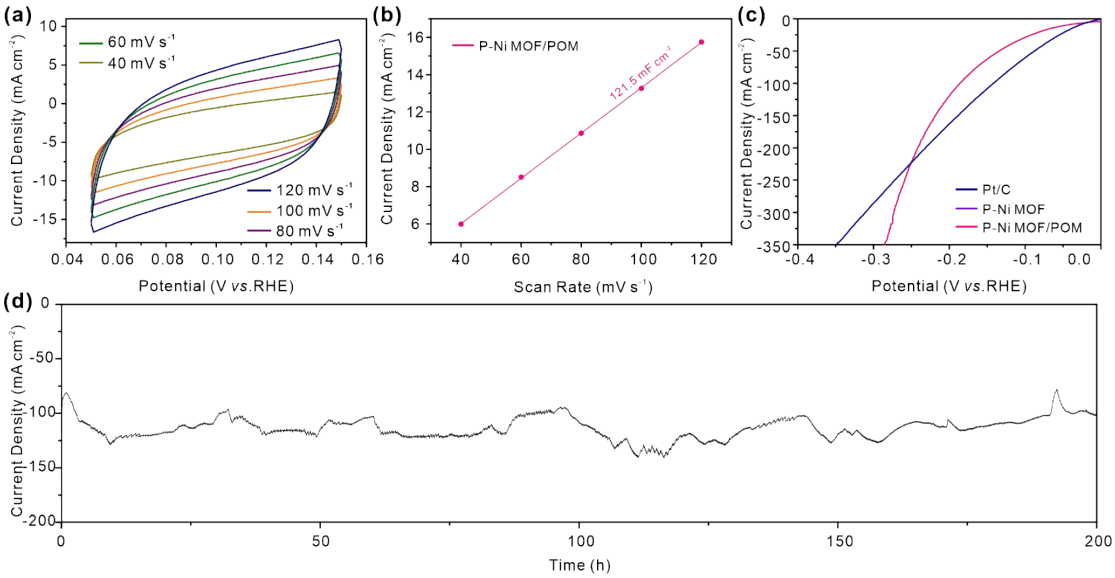


**Fig. S32.** (a) CV curves of P-Ni MOF/POM in the double layer capacitive region at different scan rates in 1.0 M KOH seawater. (b) Current density differences plotted against scan rates and (c) LSV curves of P-Ni MOF and P-Ni MOF/POM in 1.0 M KOH seawater. (d) The HER stability test of P-Ni MOF/POM in 1.0 M KOH seawater. The activity fluctuation is caused by the temperature change during day and night test.

**Reference**


1. G. Kresse and J. Hafner, *Physical Review B*, 1993, 47, 558.
2. G. Kresse and J. Furthmüller, *Physical Review B*, 1996, 54, 11169.
3. G. Kresse and J. Furthmüller, *Computational Materials Science*, 1996, 6, 15.
4. B. A. Ivanov and E. V. Tartakovskaya, *Physical Review Letters*, 1996, 77, 386.
5. P. E. Blöchl, *Physical Review B*, 1994, 50, 17953.
6. G. Kresse and D. Joubert, *Physical Review B*, 1999, 59, 1758.
7. K. Momma and F. Izumi, *Journal of Applied Crystallography*, 2011, 44, 1272.